Implicit and Semi-implicit Numerical Schemes for the Gradient Flow of the Formation of Biological Transport Networks

Di Fang, Shi Jin, Peter Markowich, Benoît Perthame

Implicit and Semi-implicit Numerical Schemes for the Gradient Flow of the Formation of Biological Transport Networks*

Di Fang†, Shi Jin‡, Peter Markowich§and Benoît Perthame¶

January 14, 2019

Abstract

Implicit and semi-implicit time discretizations are developed for the Cai-Hu model describing the formation of biological transport networks. The model couples a nonlinear elliptic equation for the pressure with a nonlinear reaction-diffusion equation for the network conductance vector. Numerical challenges include the nonlinearity and the stiffness, thus an explicit discretization puts severe constraints on the time step. We propose an implicit and a semi-implicit discretizations, which decays the energy unconditionally or under a condition independent of the mesh size respectively, as will be proven in 1D and verified numerically in 2D.

1 Introduction

Biological transport networks have drawn extensive research interests due to their ubiquitous existence in living organisms and rich phenomenon observed in nature, two common examples of which are the leaf venations and blood flow. It has been hypothesized in the literature that the branching structures of the network is governed by an optimization of the energy consumption of the living system, as a consequence of natural selection (see for example [22, 19, 17, 6, 3, 7]). However, the internal mechanism may appear rather counter-intuitive from a biological point of view, simply due to the global nature of the optimization approach in general. One naturally questions how one blood vessel, for example, with only the "knowledge" of local information, is able to participate in the global energy optimization task of the entire network. The link in between was made transparent by Hu and Cai in 2013 [15]. In their work, a global energy

*Research supported by NSF grants no. DMS-1522184, DMS-1107291: RNMS KI-Net, and NSFC grant No. 31571071.

†Department of Mathematics, University of Wisconsin-Madison, Madison, WI 53706, USA (di@math.wisc.edu).

‡School of Mathematical Sciences, Institute of Natural Sciences, MOE-LSC and SHL-MAC, Shanghai Jiao Tong University, Shanghai 200240, China (shijin-m@sjtu.edu.cn)

§Mathematical and Computer Sciences and Engineering Division, King Abdullah University of Science and Technology, Thuwal 23955-6900, Kingdom of Saudi Arabia; Faculty of Mathematics, University of Vienna, Oskar-MorgensternPlatz 1, 1090 Vienna, Austria (peter.markowich@kaust.edu.sa; peter.markowich@univie.ac.at)

¶Sorbonne Université, Université Paris-Diderot SPC, CNRS, INRIA, Laboratoire Jacques-Louis Lions, F-75005 Paris, France (Benoit.Perthame@sorbonne-universite.fr).

functional approach is suggested considering both material and metabolism costs, but nevertheless the corresponding gradient flow ends up driven by the wall shear stress on the tube walls, which is a local information and has been observed in experiments that can be sensed by the tissue [23, 18, 20]. This model unifies the global picture with the local one, and is referred to later as the *Cai-Hu model*. The original Cai-Hu model is in ODE form, which unfortunately cannot describe the growth or initiation of a network. A generalized PDE version is henceforth proposed and studied in [13, 14, 1, 11, 4, 12]. To aim at the understanding of the growth and formation of these biological networks, we consider the PDE version in this work, which is in fact a lot more challenging in terms of numerical simulations.

In the PDE model, one has a coupled system in terms of the conductance vector $m(t,x) \in \mathbb{R}^d$ (with space dimension $d \leq 2$) whose direction coincides with the allowable flow direction and whose modulus indicates how strongly the tissue passes the flow at position x, and the pressure $p(t,x) \in \mathbb{R}$ as follows:

$$-\nabla \cdot [(r(x)I + m \otimes m)\nabla p] = S, \tag{1.1}$$

$$\frac{\partial m}{\partial t} = D^2 \Delta m + c^2(\nabla p \otimes \nabla p)m - \alpha |m|^{2(\gamma-1)} m, \tag{1.2}$$

where $r(x)$ denotes the background permeability, I is the identity matrix, $S(x)$ is the distribution of fluid sources, $D > 0$ the diffusive constant (usually very small), $c > 0$ the activation constant driving the network adaptation, $\alpha > 0$ is the metabolic constant, and $\gamma \in [1/2, 1]$ is the metabolic rate of the bio-organism according to Murray's Law [21]. To be specific, it has been shown that for blood vessels, $\gamma = 1/2$ while $\gamma \in (1/2, 1]$ for leaf venation [15]. Notice that choosing the time scale allows to fix a parameter (for instance $\alpha = 1$ as later). Also note that the relationship between the pressure $p(t,x)$ and the conductivity vector $m(t,x)$ follows Darcy's Law in porous media written as the Poisson equation (1.1), where $r(x)I + m \otimes m$ is the permeability tensor. The second equation (1.2) is a reaction diffusion equation derived as a gradient flow by minimizing the energy cost functional consumed by the system. Now let us make explicit the total energy functional

$$\mathcal{E}(m) := \frac{1}{2} \int_\Omega (D^2 |\nabla m|^2 + \frac{\alpha}{\gamma} |m|^{2\gamma} + c^2 |m \cdot \nabla p[m]|^2 + c^2 r(x) |\nabla p[m]|^2)\, dx, \tag{1.3}$$

where $p[m]$ is the unique solution of the Poisson equation (1.1) subject to appropriate boundary conditions, the first term represents the diffusive energy, the second the metabolic cost consumed by the network (according to the celebrated Murray's Law in mathematical biology) to keep the tissue alive, and the last two terms correspond to the energy consumption incurred by the fluid itself – the former for the network while latter for the background. Again the pressure $p(t,x)$ here is given according to Kirchoff's law (1.1), where the flux follows Darcy's Law. We point out that this is clearly a non-convex optimization problem in general, where the first two terms are the convex part in the physical cases $\gamma \geq 1/2$ while the coupling with the Poisson equation gives rise to the non-convexity. We remark that the reaction term in (1.2) illustrates a competition between the contribution by activation forces (by flow inside the network) $c^2(\nabla p \otimes \nabla p)m$ and the metabolic part $-\alpha |m|^{2(\gamma-1)} m$. And it is exactly this competition that gives rise to interesting branching phenomena and nontrivial equilibria.

Although model (1.1)-(1.2) may appear "standard" at a first glance in the form of a Poisson equation coupled with an diffusion-reaction equation, it is by no means easy to compute in

practice. The major numerical difficulty of this system lies in the stiffness of basically all terms in (1.2). Unlike the rather standard reaction-diffusion equation (such as the Allen-Cahn equation) where the reaction term is smooth, we point out that with the physical parameter $\gamma \in (1/2, 1)$, the activation term $\alpha|m|^{2(\gamma-1)}m$ in (1.2) is not smooth and in fact stiff since m can be close to zero (to be made more transparent in later discussions with the 1D case). This feature makes our problem more difficult than well-studied reaction diffusion equations where the smoothness of the reaction term is guaranteed. Hence a direct application of the currently-developed tricks for reaction diffusion equations, such as linear penalization [9, 8, 10] and its resulting Integration Factor (IF) method or Exponential Time Differencing (ETD) method [9, 8] remain not clear. Before proceeding any further we summarize the main numerical difficulties of this system as follows

1. The diffusion term $D^2\Delta m$ is stiff as in any reaction-diffusion system. This is actually not a real difficulty at all, since the stiffness of the diffusion can be removed by treating the term exactly or implicitly. Different approximations on the temporal integral involving reaction term in this approach result in either Integration Factor (IF) methods or Exponential Time Differencing (ETD) methods [9, 8].

2. The metabolism term $|m|^{2(\gamma-1)}m$ is nonlinear and non-differentiable in general for physical most relevant cases $\frac{1}{2} \leq \gamma \leq 1$, and is also stiff since m can be close to zero. This term is in fact much harder to treat than the diffusion.

3. The activation matrix (in 2D) $c^2\nabla p \otimes \nabla p$ has eigenvalues 0 and $c^2|\nabla p|^2$, which makes the activation term stiff when $|\nabla p|$ is large. This is precisely the case 'inside' the network.

In the literature, a number of efforts have been devoted to construct effective numerical schemes for this system. [14] and [1] develop numerical schemes with only the diffusion term implicit formulated in either a forward Euler or a Crank Nicolson fashion and other terms explicit, and [2] presents a time-splitting strategy, where the stability of the former remain unclear and the latter has severe time-step constraints due to the stiffness. The goal of this paper is to develop efficient implicit and semi-implicit schemes with good stability properties. First, to effectively take care of the stiffness, we propose a fully implicit scheme for both 1D and 2D Cai-Hu models. For 1D, we prove that the energy dissipation equation is preserved which gives the unconditional stability of the implicit solver. However, as any implicit solver to nonlinear equations, the scheme gives rise to a nonlinear algebraic problem and hence requires the Newton iterations, which makes the implementation for multi-dimensional cases utterly costly and complicated. Even worse, the convergence of the Newton solver becomes unclear for the 2D case. To achieve a practical algorithm with only linear algebraic solvers needed, semi-implicit treatment is desired. However, as is well known, unlike the fully implicit treatment, it is usually difficult to construct a semi-implicit solver that still decays the energy functional (physical energy) of the gradient flow. As the second and main part, we propose a semi-implicit scheme for the Cai-Hu model in both 1D and 2D that does not result in nonlinear algebraic problems. Moreover, we prove for 1D that this scheme indeed decays the physical energy as long as a condition independent of the mesh size is satisfied. With this new solver, one only needs to deal with linear algebraic problems that can be easily solved either by conjugate gradient (CG) or preconditioned conjugate gradient (PCG). This makes the computation in 2D efficient and feasible. Though we only prove the decay of

the physical energy in 1D for the semi-implicit solver, numerically one observes that the physical energy decays in time for both 1D and 2D cases.

The rest of the paper is organized as follows: In Section 2, we briefly revisit the 1D Cai-Hu model, and propose an implicit algorithm whose unconditional stability is proved. Motivated by the practical calculation for higher dimensional cases, we henceforth propose a semi-implicit scheme, and prove that it decays the physical energy provided the stability condition is satisfied in 1D. Section 3 presents both the fully implicit and semi-implicit schemes for 2D in analogy to the 1D case. In Section 4, numerical tests are conducted in 1D with both the implicit and semi-implicit solvers, and 2D with the semi-implicit one. We observe numerically in both cases the energy decreases in time. The 2D examples present branching phenomena as occurred in leaf venations in nature. Section 5 contains conclusions.

2 The 1D Cai-Hu Model and Numerical Approximations

2.1 The 1D Cai-Hu Model

As has been shown in [14], the *1D Cai-Hu model* has the form

$$\partial_t m - D^2 \partial_{xx}^2 m = \left(\frac{c^2 B(x)^2}{(1+m^2)^2} - |m|^{2(\gamma-1)} \right) m \tag{2.1}$$

with proper boundary conditions (see [14] for the detailed derivation), where the parameters are already chosen as $r(x) = \alpha = 1$ for simplicity and $B(x)$ is the given function

$$B(x) := \int_0^x S(y) dy.$$

The energy in the 1D setting is then simplified as

$$\mathcal{E}(m) = \frac{1}{2} \int_\Omega D^2 |\partial_x m|^2 + \frac{1}{\gamma} |m|^{2\gamma} + \frac{c^2 B(x)^2}{1+m^2} dx. \tag{2.2}$$

As has been pointed out in the introduction, the nonlinear reaction term is also stiff. To see it, simply defines

$$H(m) = \left(\frac{c^2 B(x)^2}{(1+m^2)^2} - |m|^{2(\gamma-1)} \right) m, \tag{2.3}$$

where $-1 \le 2(\gamma-1) \le 0$, since $\frac{1}{2} \le \gamma \le 1$, and

$$H'(m) = \begin{cases} c^2 B(x)^2 \frac{1-3m^2}{(1+m^2)^3} - \frac{2\gamma-1}{|m|^{2(1-\gamma)}}, & \text{if } m \neq 0, \\ -\infty, & \text{if } m = 0. \end{cases} \tag{2.4}$$

Note that $|H'(m)|$ is very large as m approaches zero.

2.2 An Implicit Treatment and Energy Decay

Consider the 1d setting in [14], namely, the interval $(0, 1)$ and homogenous Neumann Boundary Conditions for m. We propose the following scheme:

$$\frac{m_j^{n+1} - m_j^n}{\Delta t} = \frac{D^2}{2\Delta x^2} \left[m_{j+1}^{n+1} - 2m_j^{n+1} + m_{j-1}^{n+1} + m_{j+1}^n - 2m_j^n + m_{j-1}^n \right] \tag{2.5}$$

$$+\frac{c^2B_j^2(m_j^{n+1}+m_j^n)}{2(1+(m_j^{n+1})^2)(1+(m_j^n)^2)}-\frac{(m_j^{n+1})^{2\gamma}-(m_j^n)^{2\gamma}}{2\gamma(m_j^{n+1}-m_j^n)}. \tag{2.6}$$

$$m_{-1}=m_1,\quad m_{N-1}=m_{N+1}.$$

Note that this scheme is second order in time, and the diffusion term is treated by the Crank-Nicolson method. We define the discrete energy as

$$E^n=\frac{1}{2}\sum_{j=1}^{M}\left[\frac{D^2}{\Delta x^2}\left(m_j^n-m_{j-1}^n\right)^2+\frac{1}{\gamma}|m_j^n|^{2\gamma}+\frac{c^2B_j^2}{1+(m_j^n)^2}\right], \tag{2.7}$$

which is a discrete analog of the energy functional (2.2). We shall prove in the following theorem that our scheme decays the discrete energy and is hence unconditionally stable.

Theorem 2.1. *The scheme* (2.6) *satisfies the discrete energy dissipation equation*

$$E^{n+1}-E^n=-\frac{1}{\Delta t}\sum_{j=1}^{M}(m_j^{n+1}-m_j^n)^2, \tag{2.8}$$

and hence decays the energy

$$E^{n+1}\le E^n. \tag{2.9}$$

Remark 2.2. This result implies that the scheme is unconditionally stable, i.e. there is no restriction on Δt. It shows the scheme preserves in the discrete fashion the energy equation given in Lemma 1 of [13]

$$\frac{d}{dt}\mathcal{E}=-\int_\Omega\left(\frac{\partial m}{\partial t}\right)^2dx. \tag{2.10}$$

In fact, one should simply view the scheme as a discretization of the energy equation.

Proof. The lemma follows a straightforward energy estimate, namely, multiply $m_j^{n+1}-m_j^n$ on both sides of the scheme (2.6) and sum over j,

$$\sum_{j=1}^{M}\frac{(m_j^{n+1}-m_j^n)^2}{\Delta t}=\text{(I)}+\text{(II)}+\text{(III)},$$

where

$$\text{(I)}=\sum_{j=1}^{M}\frac{D^2}{2\Delta x^2}\left(m_{j+1}^{n+1}-2m_j^{n+1}+m_{j-1}^{n+1}+m_{j+1}^n-2m_j^n+m_{j-1}^n\right)(m_j^{n+1}-m_j^n),$$

$$\text{(II)}=\sum_{j=1}^{M}\frac{c^2B_j^2}{2}\frac{(m_j^{n+1})^2-(m_j^n)^2}{(1+(m_j^{n+1})^2)(1+(m_j^n)^2)},\quad \text{(III)}=-\sum_{j=1}^{M}\frac{1}{2\gamma}\left[(m_j^{n+1})^{2\gamma}-(m_j^n)^{2\gamma}\right].$$

It follows from summation by parts that

$$\sum_j\left(m_{j+1}^{n+1}-2m_j^{n+1}+m_{j-1}^{n+1}\right)m_j^{n+1}=\sum_j\left(m_{j+1}^{n+1}-m_j^{n+1}\right)m_j^{n+1}-\sum_j\left(m_j^{n+1}-m_{j-1}^{n+1}\right)m_j^{n+1} \tag{2.11}$$

$$= -\sum_j \left(m_j^{n+1} - m_{j-1}^{n+1}\right)^2. \tag{2.12}$$

Similarly applying summation by parts to other terms, one finds

$$\begin{aligned}
\text{(I)} =& \frac{D^2}{2\Delta x^2}\sum_{j=1}^{M}\left(m_{j+1}^{n+1} - 2m_j^{n+1} + m_{j-1}^{n+1}\right)m_j^{n+1} - \frac{D^2}{2\Delta x^2}\sum_{j=1}^{M}\left(m_{j+1}^{n} - 2m_j^{n} + m_{j-1}^{n}\right)m_j^{n} \\
&+ \frac{D^2}{2\Delta x^2}\sum_{j=1}^{M}\left(m_{j+1}^{n} - 2m_j^{n} + m_{j-1}^{n}\right)m_j^{n+1} - \frac{D^2}{2\Delta x^2}\sum_{j=1}^{M}\left(m_{j+1}^{n+1} - 2m_j^{n+1} + m_{j-1}^{n+1}\right)m_j^{n} \\
=& -\frac{D^2}{2\Delta x^2}\sum_j \left(m_j^{n+1} - m_{j-1}^{n+1}\right)^2 + \frac{D^2}{2\Delta x^2}\sum_j \left(m_j^{n} - m_{j-1}^{n}\right)^2.
\end{aligned}$$

A simple calculation shows

$$\begin{aligned}
\text{(II)} =& \sum_{j=1}^{M}\frac{c^2B_j^2}{2}\frac{(m_j^{n+1})^2 - (m_j^n)^2}{(1+(m_j^{n+1})^2)(1+(m_j^n)^2)} \\
=& -\frac{1}{2}\sum_{j=1}^{M}\frac{c^2B_j^2}{1+(m_j^{n+1})^2} + \frac{1}{2}\sum_{j=1}^{M}\frac{c^2B_j^2}{1+(m_j^n)^2}.
\end{aligned}$$

Hence,

$$\text{(I)} + \text{(II)} + \text{(III)} = -E^{n+1} + E^n,$$

which completes the proof. □

In numerical implementations, we use the Newton method to solve the implicit algebraic equation (2.6) in every time step. Note that supposing $D = 0$, then the algebraic equation has only one root, and sufficiently away from 0 the function in consideration is actually monotone. Numerically, the Newton iteration converges just in a few steps taking the initial guess sufficiently away from 0.

2.3 A Semi-implicit Treatment and Energy Decay

To avoid the nonlinear Newton solver, which may become impractical for higher dimension, we propose the following semi-implicit treatment in preparation for the 2D practical simulations.

$$\frac{m_j^{n+1} - m_j^n}{\Delta t} - \frac{D^2}{\Delta x^2}\left[m_{j+1}^{n+1} - 2m_j^{n+1} + m_{j-1}^{n+1}\right] = \frac{c^2B(x)^2}{\left(1+(m_j^n)^2\right)^2}m_j^n - |m_j^n|^{2(\gamma-1)}m_j^{n+1}, \tag{2.13}$$

$$m_{-1} = m_1, \quad m_{N-1} = m_{N+1}.$$

Note that in (2.13), the activation part on the right hand side is treated fully explicitly, while the metabolic term is treated in a semi-implicit fashion. Since $|m_j^n|^{2(\gamma-1)}$ is strictly positive, this term plays the role of stabilizing the scheme. Moreover, one only needs to invert a tri-diagonal matrix where standard fast algorithms can be used. In the following theorem, we establish the conditional stability of the semi-implicit solver in the semi-discrete set-up which guarantees the physical energy does not increase. Note that the semi-discretization is used for a clear presentation, the fully-discrete stability should be similar, which is omitted here.

Theorem 2.3. *Assume $B \in L^\infty$, consider the semi-implicit scheme* (2.13) *in the semi-discrete set-up, i.e.,*

$$\frac{m^{n+1}-m^n}{\Delta t} - D^2\partial_{xx}m^{n+1} = \frac{c^2B(x)^2}{\left(1+(m^n)^2\right)^2}m^n - |m^n|^{2(\gamma-1)}m^{n+1}, \tag{2.14}$$

then the physcial energy as defined in (2.2) *decays*

$$\mathcal{E}(m^{n+1}) \le \mathcal{E}(m^n),$$

provided the condition

$$c^2\|B^2\|_\infty \Delta t \le 2, \tag{2.15}$$

is satisfied.

Proof. Denote

$$f(m) = \frac{c^2B(x)^2}{(1+m^2)^2}m, \quad F(m) = \frac{c^2B(x)^2}{2(1+m^2)},$$

then clearly one has $F'(m) = -f(m)$ and

$$|f'(m)| = c^2B(x)^2\left|\frac{1-3m^2}{(1+m^2)^3}\right| \le c^2\|B^2\|_\infty. \tag{2.16}$$

In the following, we use $\langle\cdot,\cdot\rangle$ to denote the inner product and $\|\cdot\|$ for the L^2 norm in Ω.

On one hand, multiplying the scheme (2.14) by $m^{n+1}-m^n$ and integrating in x, one obtains

$$\begin{aligned}\frac{1}{\Delta t}\|m^{n+1}-m^n\|^2 + \frac{D^2}{2}\|\partial_x m^{n+1}\|^2 - \frac{D^2}{2}\|\partial_x m^n\|^2 + \frac{D^2}{2}\|\partial_x m^{n+1}-\partial_x m^n\|^2 \\ = \langle f(m^n), m^{n+1}-m^n\rangle - \int_\Omega |m^n|^{2\gamma-2}\big((m^{n+1})^2 - m^{n+1}m^n\big)dx,\end{aligned} \tag{2.17}$$

where integration by parts and the equality $\langle a-b, a\rangle = \frac{1}{2}\|a\|^2 - \frac{1}{2}\|b\|^2 + \frac{1}{2}\|a-b\|^2$ are used. On the other hand, it holds that

$$\begin{aligned}\mathcal{E}(m^{n+1}) - \mathcal{E}(m^n) = \frac{D^2}{2}\|\partial_x m^{n+1}\|^2 - \frac{D^2}{2}\|\partial_x m^n\|^2 + \int_\Omega \frac{1}{2\gamma}|m^{n+1}|^{2\gamma} - \frac{1}{2\gamma}|m^n|^{2\gamma}dx \\ + \int_\Omega F(m^{n+1}) - F(m^n)dx,\end{aligned} \tag{2.18}$$

by the definition of the physical energy (2.2). Notice that

$$F(m^{n+1}) - F(m^n) = -f(m^n)(m^{n+1}-m^n) - \int_{m^n}^{m^{n+1}} f'(\tau)(m^{n+1}-\tau)d\tau,$$

and hence combining with (2.17), we have

$$\begin{aligned}&\mathcal{E}(m^{n+1}) - \mathcal{E}(m^n) + \frac{1}{\Delta t}\|m^{n+1}-m^n\|^2 + \frac{D^2}{2}\|\partial_x m^{n+1}-\partial_x m^n\|^2 \\ &= -\int_\Omega |m^n|^{2\gamma-2}\big((m^{n+1})^2 - m^{n+1}m^n\big) - \frac{1}{2\gamma}|m^{n+1}|^{2\gamma} + \frac{1}{2\gamma}|m^n|^{2\gamma}dx - \int_\Omega\int_{m^n}^{m^{n+1}} f'(\tau)(m^{n+1}-\tau)d\tau dx \\ &:= I_1 + I_2\end{aligned}$$

By (2.16), clearly

$$I_2 \le \frac{1}{2}c^2\|B^2\|_\infty\|m^{n+1}-m^n\|^2.$$

Next, we shall show that $I_1 \le 0$.

Case 1: If $m^{n+1}m^n \ge 0$, it suffices to show that the function

$$G(x,y) = x^{2\gamma-2}y^2 - x^{2\gamma-1}y - \frac{1}{2\gamma}y^{2\gamma} + \frac{1}{2\gamma}x^{2\gamma} \ge 0 \tag{2.19}$$

for all $x, y \ge 0$. (Note that I_1 corresponds to the case when $x = |m^n|$ and $y = |m^{n+1}|$.) Though one could prove the result by proving the minimum of $G(x,y)$ is no less than 0, an easier way is to use the homogeneity of the inequality and convert the problem into a single variable function. To be specific, note that

$$G(x,y) = x^{2\gamma}\Big((\frac{y}{x})^2 - \frac{y}{x} - \frac{1}{2\gamma}(\frac{y}{x})^{2\gamma} + \frac{1}{2\gamma}\Big). \tag{2.20}$$

Denote $z = y/x \ge 0$, it suffices to show that

$$A(z) = z^2 - z - \frac{1}{2\gamma}z^{2\gamma} + \frac{1}{2\gamma} \ge 0$$

for all $z \ge 0$. It clearly holds for $z = 0$ and for $\gamma = 1/2$ respectively, hence we only need to consider $z > 0$ and $\gamma \in (1/2, 1)$. Straightforward computation gives

$$A'(z) = 2z - 1 - z^{2\gamma-1}, \quad A''(z) = 2 - \frac{2\gamma-1}{z^{2-2\gamma}},$$

where $A''(z)$ is monotone increasing with a unique zero at $z = (\frac{2}{2\gamma-1})^{2\gamma-2} := z_0$, which means $A'(z)$ decreases in $(0, z_0)$ and increases in (z_0, ∞). On one hand, one has $A'(0) = -1 < 0$, which implies that $A'(z)$ has at most one zero. On the other hand, $z = 1$ is clearly a critical point, and therefore is the unique critical point of $A(z)$. One could easily check the second derivatives and the limits on the boundary to see that the critical point $z = 1$ is the global minimum. It follows that

$$A(z) \ge A(1) = 0, \quad G(x,y) \ge 0.$$

Case 2: When $m^{n+1}m^n < 0$, it suffices to show that

$$\tilde{G}(x,y) = x^{2\gamma-2}y^2 + x^{2\gamma-1}y - \frac{1}{2\gamma}y^{2\gamma} + \frac{1}{2\gamma}x^{2\gamma} \ge 0$$

for all $x, y \ge 0$, which clearly holds since

$$\tilde{G}(x,y) = G(x,y) + 2x^{2\gamma-1}y \ge 0.$$

In summary, we have

$$\mathcal{E}(m^{n+1}) - \mathcal{E}(m^n) + \frac{D^2}{2}\|\partial_x m^{n+1} - \partial_x m^n\|^2 \le (\frac{c^2\|B^2\|_\infty}{2} - \frac{1}{\Delta t})\|m^{n+1} - m^n\|^2 \le 0,$$

where the stability condition (2.15) is used. This completes the proof.

□

3 The 2D Cai-Hu Model and Numerical Schemes

The ideas developed in the 1D case can be extended to treat the spatially discretized 2D Cai-Hu model when set on a rectangular grid. For completeness, we present both the fully implicit and implicit-explicit schemes.

3.1 An Implicit Approach and Energy Decay

Similar as the 1D case, an implicit scheme can be constructed as

$$-\nabla_h \cdot \left[\frac{r}{2}\left(\nabla_h p^{n+1} + \nabla_h p^n\right) + \frac{1}{4}\left(m^{n+1}\cdot\nabla_h p^{n+1} + m^n \cdot \nabla_h p^n\right)\left(m^{n+1}+m^n\right)\right] = S, \tag{3.1}$$

$$\begin{aligned}\frac{m_l^{n+1}-m_l^n}{\Delta t} = \frac{D^2}{2}\nabla_h^2\left(m_l^{n+1}+m_l^n\right) + \frac{c^2}{4}\left(m^{n+1}\cdot\nabla_h p^{n+1} + m^n\cdot\nabla_h p^n\right)\left(\nabla_h p_l^{n+1} + \nabla_h p_l^n\right)\\ -\frac{\alpha}{2\gamma}\frac{|m^{n+1}|^{2(\gamma-1)}(m_l^{n+1})^2 - |m^n|^{2(\gamma-1)}(m_l^n)^2}{\left(m_l^{n+1}-m_l^n\right)},\end{aligned} \tag{3.2}$$

where the subscript $l = 1, 2$ labels the l-th component of the vector m or $\nabla_h p$; the spatial discretizations are all performed at the grid point with index-pair (k, j) and hence spatial indices are omitted for simplicity; and ∇_h^2 denotes the discretized Laplacian operator, and hence the diffusion term is treated in a Crank-Nicolson matter (similarly as 1D case). This scheme is clearly second order in time.

However, this scheme gives rise to an nonlinear algebra problem, which in practice is very difficult to solve. Note that a direct application of the Newton iteration may fail to converge depending on initial guesses. Hence in the next section, we propose a more practical numerical method.

3.2 A Semi-implicit Scheme

The key goal here is to avoid a nonlinear algebraic problem which requires the Newton iterations, in which case hopefully one only deals with a linear algebra problem that provides enough efficiency in practical calculation. Following the semi-implicit idea for the 1D Cai-Hu model, we propose the following scheme for multi-dimensional cases:

$$-\mathcal{D}_1 \cdot [(rI + m^n \otimes m^n)\mathcal{D}_1 p^{n+1}] = S, \tag{3.3}$$

$$\begin{aligned}\frac{m_1^{n+1}-m_1^n}{\Delta t} &= D^2\mathcal{D}_2 m_1^{n+1} + c^2\left((\mathcal{D}_x p^{n+1})^2 m_1^n + \mathcal{D}_x p^{n+1}\mathcal{D}_y p^{n+1} m_2^n\right) - \alpha|m^n|^{2(\gamma-1)}m_1^{n+1},\\ \frac{m_2^{n+1}-m_2^n}{\Delta t} &= D^2\mathcal{D}_2 m_2^{n+1} + c^2\left((\mathcal{D}_y p^{n+1})^2 m_2^n + \mathcal{D}_x p^{n+1}\mathcal{D}_y p^{n+1} m_1^n\right) - \alpha|m^n|^{2(\gamma-1)}m_2^{n+1},\end{aligned} \tag{3.4}$$

where $\mathcal{D}_x$ and $\mathcal{D}_y$ denote the spatial discretizations in x and y directions, respectively, which could be chosen as either the forward difference or the central difference, $\mathcal{D}_1 = (\mathcal{D}_x, \mathcal{D}_y)$, and $\mathcal{D}_2 = \mathcal{D}_x^2 + \mathcal{D}_y^2$. Note that similarly to the 1D scheme (2.13), the diffusion term is treated implicitly, the metabolism term semi-implicitly and the activation term explicitly in the sense that

the pressure p^{n+1} used here is computed from the Poisson equation (3.3) using the information of m^n. This semi-implict scheme is a 2D version of scheme (2.13) that has been proven to decay the physical energy in 1D, and is efficient in actual computations, since the semi-implicit treatment of the last term in (3.4) helps to stabilize the whole procedure and create positive definite matrices to be inverted. For numerical tests, we use the staggered grids, as is widely used in computational fluid dynamics to avoid the famous "checkerboard" problem.

4 Numerical Results

We now illustrate the theoretical results with numerical simulations. We compare the semi-implicit scheme and the fully implicit which is more complex due to Newton iterations but avoids the restriction on time steps. We pay a special attention to the decay of energy as it holds for the continuous model, and on the ability of the scheme to generate patterns.

4.1 The 1D Cai-Hu Model

In this section, we present our numerical results of the 1D Cai-Hu model (2.1) using the implicit solver (2.6) and the semi-implicit scheme (2.13), respectively. Denote the nonlinear system of equations resulting from the implicit scheme as

$$F(m^{n+1}) := \frac{m_j^{n+1}-m_j^n}{\Delta t} - \frac{D^2}{2\Delta x^2}\left[m_{j+1}^{n+1} - 2m_j^{n+1} + m_{j-1}^{n+1} + m_{j+1}^n - 2m_j^n + m_{j-1}^n\right] - \frac{c^2 B_j^2 (m_j^{n+1}+m_j^n)}{2(1+(m_j^{n+1})^2)(1+(m_j^n)^2)} + \frac{(m_j^{n+1})^{2\gamma} - (m_j^n)^{2\gamma}}{2\gamma(m_j^{n+1}-m_j^n)} = 0, \tag{4.1}$$

where $F : \mathbb{R}^N \to \mathbb{R}^N$. The Newton method reads

$$J_F\left(m^{n+1}(k)\right)\left(m^{n+1}(k+1) - m^{n+1}(k)\right) = -F\left(m^{n+1}(k)\right),$$

with $J_F(m^{n+1})$ as the $N \times N$ Jacobian matrix of F and k as the k-th step of iteration. In order to solve this linear system, the Thomas algorithm [5] is implemented since the Jacobian is a tri-diagonal matrix.

Example 4.1 (1D Extinction of Solutions)**.** It has been shown in Lemma 4 of [14] that for $1/2 \le \gamma \le 1$, the initial data $m^0 \in L^\infty(0,1)$ and the parameters satisfying

$$c\|B(x)\|_{L^\infty} \le Z_\gamma := \frac{2}{\gamma+1}\left(\frac{1-\gamma}{1+\gamma}\right)^{\frac{\gamma-1}{2}},$$

one has the extinction of solutions, namely, the solution converges to zero as $t \to \infty$. In other words, the solution converges to zero in infinite time for $1/2 \le \gamma \le 1$ (in contrast to the case $-1 \le \gamma < 1/2$ where there exists a finite break down time). In this example, we try to observe the vanishing effect numerically. Consider $\gamma = 0.75$ corresponding to the leaf venation case, $D = 0.01$, $cB(x) = Z_\gamma/2$, and initial datum as

$$m(0,x) = 10(\sin(2\pi x) + 1)\cos(2\pi x) - 3, \tag{4.2}$$

which is plotted in Fig. 1a. We choose this initial datum so that it is a bit more complicated than simple algebraic functions, and here one has different combinations of monotonicity and convexity

in the sub-intervals. Both the implict and semi-implict solvers are implemented with $\Delta t = 0.01$ and $\Delta x = 0.005$ until the final time $T = 10$. We first show the results of the implicit solver: Fig 1 plots the solutions at various time $t = 0, 2, 5, 10$ and the discrete physical energy defined in (2.7). It can be seen that the discrete physical energy decays throughout the simulation in time as is proved in Theorem 2.1. Next, the solutions computed by the semi-implicit scheme at different time and its discrete physical energy are plotted in Fig. 2. In the numerics one indeed can see the decay of the discrete physical energy as is proved in Theorem 2.3. In both methods, the solution converges finally to zero and we numerically recover the theoretical results proved in Lemma 4 of [14].

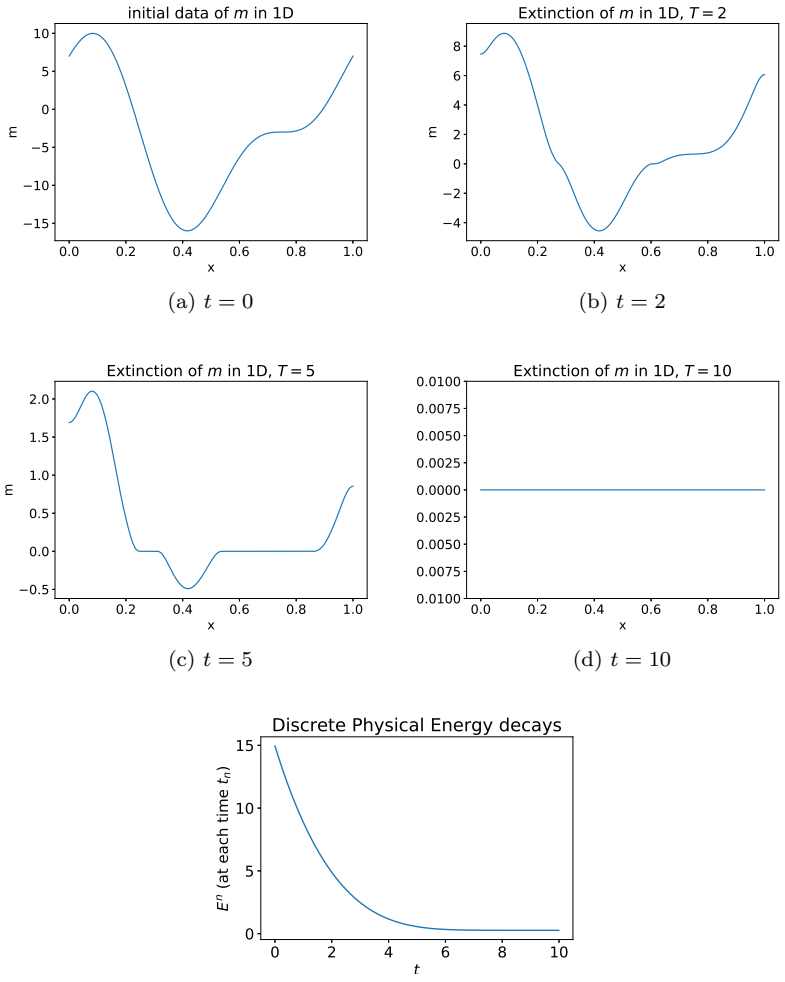

(a) $t = 0$ (b) $t = 2$

(c) $t = 5$ (d) $t = 10$

(e) Discrete Physical Energy

Figure 1: Example 4.1 computed by the implicit solver: the solution m at different times $t = 0, 2, 5, 10$. It can be seen that the solution converges to 0 eventually, and the discrete physical energy decreases in time.

Example 4.2 (1D Non-trivial Equilibrium)**.** In this example, we want to consider the solution with non-trivial (non-vanishing) equilibrium. First, consider the 1D Cai-Hu model (2.1) with

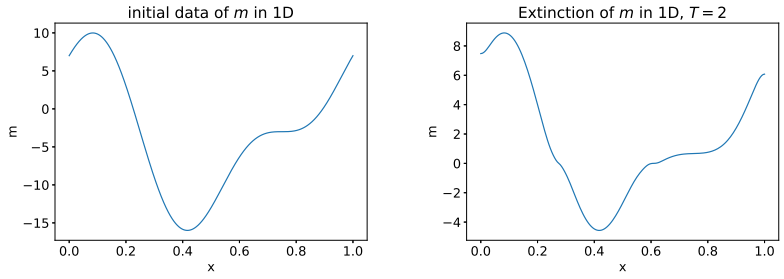

(a) $t = 0$

(b) $t = 2$

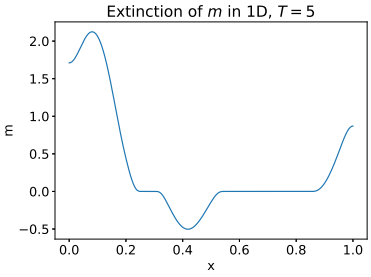

(c) $t = 5$

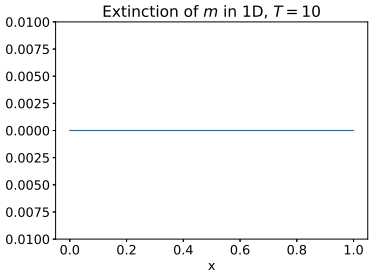

(d) $t = 10$

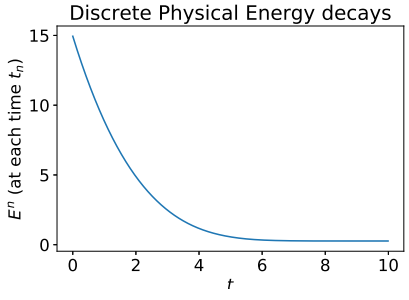

(e) Discrete Physical Energy

Figure 2: Example 4.1 computed by the semi-implicit solver: the solution m at different times $t = 0, 2, 5, 10$. It can be seen that the solution converges to 0 eventually, and the discrete physical energy decreases.

parameters

$$D = 0.01, \quad cB(x) = 10, \quad \gamma = 0.75,$$

which corresponds to the leaf venation case with the initial datum as (4.2), and compute the 1D model until the final time $T = 20$, using both the implicit and semi-implicit methods with $\Delta t = 0.01$ and $\Delta x = 0.005$. The numerical results are plotted in Fig. 3. For both schemes, we observe the decay of the discrete physical energy. Next, we change the diffusion parameter

$$D = 0.001,$$

and repeat above tests. It can be seen in Fig. 4, the decay of discrete energy can still be observed.

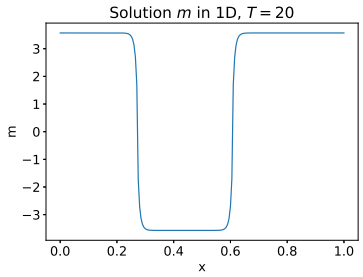

(a) Implicit scheme: m at $t = 20$

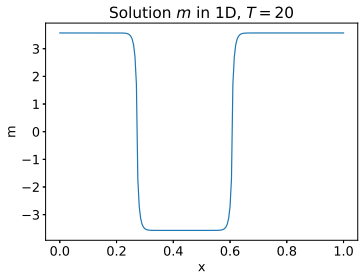

(b) Semi-implicit scheme: m at $t = 20$

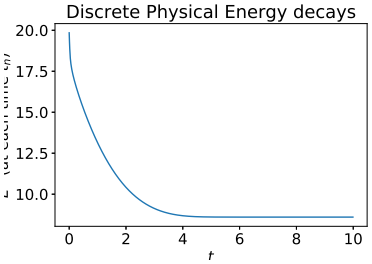

(c) Implicit scheme: discrete energy

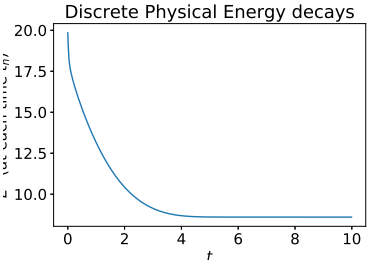

(d) Semi-implicit scheme: discrete energy

Figure 3: Example 4.2 with $D = 0.01$. Left panel: computed by the implicit solver; right panel: computed by semi-implicit solver. The equilibrium does not vanish and the discrete physical energy is observed to decay in time.

4.2 The 2D Cai-Hu Model

In this section, we present a number of numerical examples for the 2D Cai-Hu model, using the semi-implicit solver. The linear algebraic problems resulting from the scheme are solved using a preconditioned conjugate gradient method. The discrete physical energy considered here is defined as $\mathcal{E}(m^n)$ at each time $t = t_n$, with $\mathcal{E}$ defined in (1.3).

Example 4.3. Consider the equation with the Neumann boundary condition for p and Dirichlet boundary condition for m. The background permeability $r(x)$ is chosen as $r(x) = 0.1$, the activation constant $c = 50$, the diffusivity $D = 0.01$, and $\alpha = 1$. We choose $\gamma = 0.75$, which corresponds to leaf venations according to [16]. The initial data and source term are given in Fig. 5.

In this example we use $\Delta t = 0.005$, and $\Delta x = \Delta y = 0.002$. We plot the long-time behavior of the system for various time $T = 20, 40, 60, 80$. To be specific, Fig. 6 shows $|m|^2$ in the log-scale, which corresponds to the structure of the leaf. Note that for $m = 0$, the log function is not defined, and hence hereafter $\log(|m|^2 + \epsilon_0)$ is plotted in numerics, where $\epsilon_0 = 4\text{e}{-16}$ is of size of machine precision. In this example, we also plot the volumetric flux u (proportional to the flow velocity in leaf venations), defined as

$$u = (rI + m \otimes m)\nabla p \tag{4.3}$$

in Fig. 7. It can be seen that the leaf venation grows as the fluid spreads, and finally achieve a tree-like structure. Numerically, we see that the discrete physical energy decays with respect to

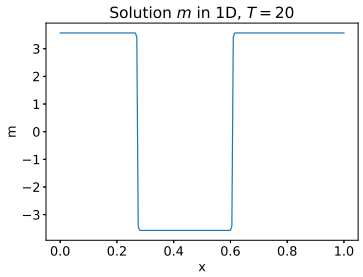

(a) Implicit scheme: m at $t = 20$

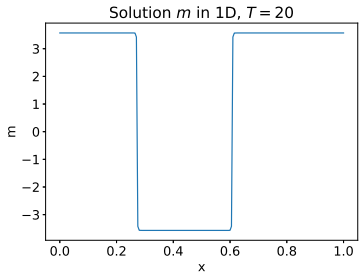

(b) Semi-implicit scheme: m at $t = 20$

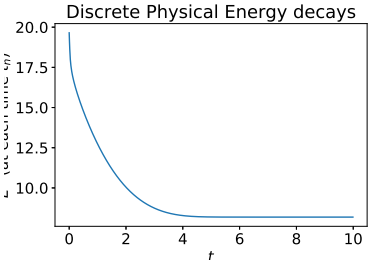

(c) Implicit scheme: discrete energy

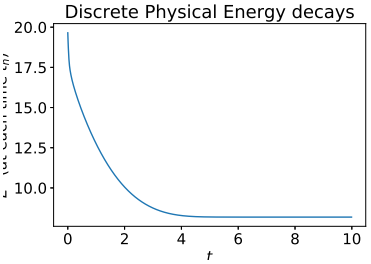

(d) Semi-implicit scheme: discrete energy

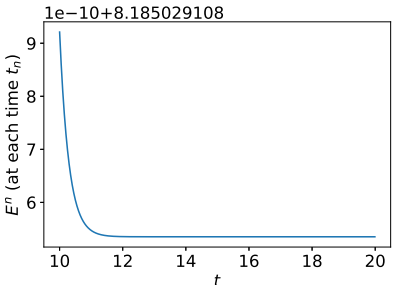

(e) Implicit scheme: zoom in of discrete energy after $t = 10$

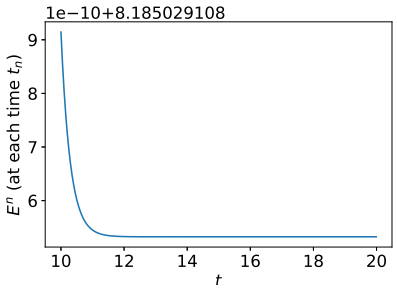

(f) Semi-implicit scheme: zoom in of discrete energy after $t = 10$

Figure 4: Example 4.2 with $D = 0.001$. Left panel: computed by the implicit solver; right panel: computed by semi-implicit solver. The equilibrium does not vanish and the discrete physical energy is observed to decay in time for both solvers.

time through out the simulation as is shown 8. In fact, in the last several steps, the energy keeps the decay behavior even if the first five decimal places in the energy value no longer change. To be specific, the last seven energy values are

$$2.40638937, 2.40638876, 2.40638813, 2.40638744, 2.40638683, 2.40638619, 2.40638551.$$

Example 4.4 (Varying D)**.** In this example, we investigate how the diffusion coefficients may affect the formation of the biological network. Consider the same set-up as in Example 4.3, but with different diffusion coefficients $D = 0.5, 0.1, 0.02, 0.005, 0.002$. The solutions are computed till time $T = 40$. It can be seen from Fig. 9 that the smaller the diffusion coefficient is, the more detailed structure the network tends to exhibit and also the faster it reaches the equilibrium.

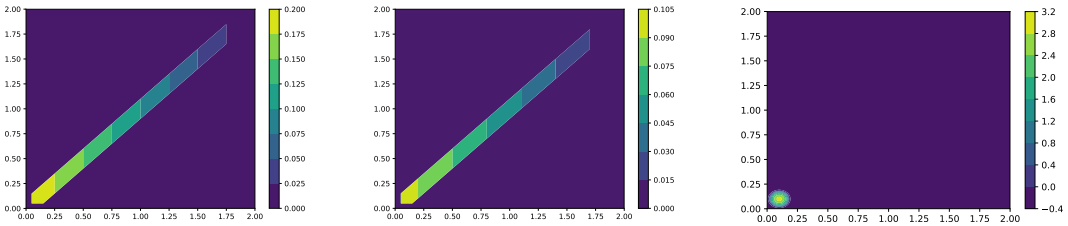

(a) $m_1(0, x, y)$ (b) $m_2(0, x, y)$ (c) $S(x, y)$

Figure 5: Plot of initial data in the (x,y) plane and the source term.

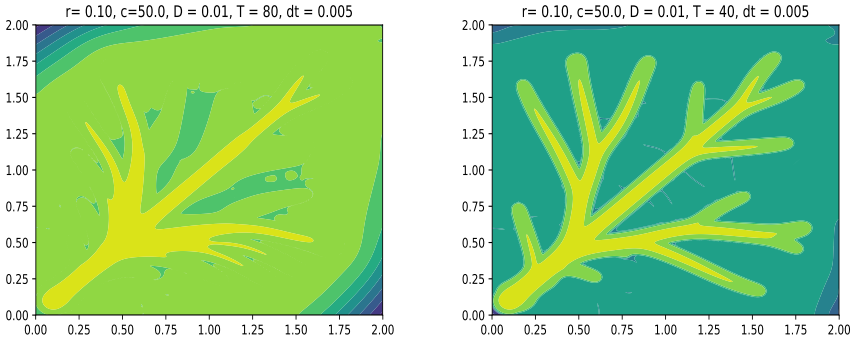

(a) $t = 20$ (b) $t = 40$

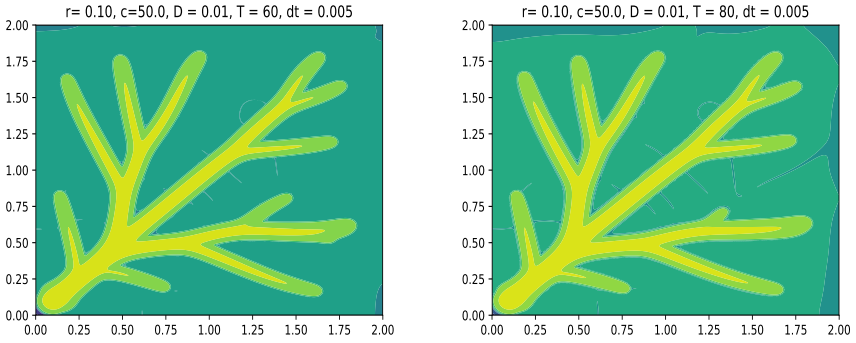

(c) $t = 60$ (d) $t = 80$

Figure 6: Example 4.3 computed by the semi-implicit solver: the leaf structure $|m|^2$ in the log scale at different times $t = 20, 40, 60, 80$. It can be seen that the flow spreads and finally achieves a tree-like structure.

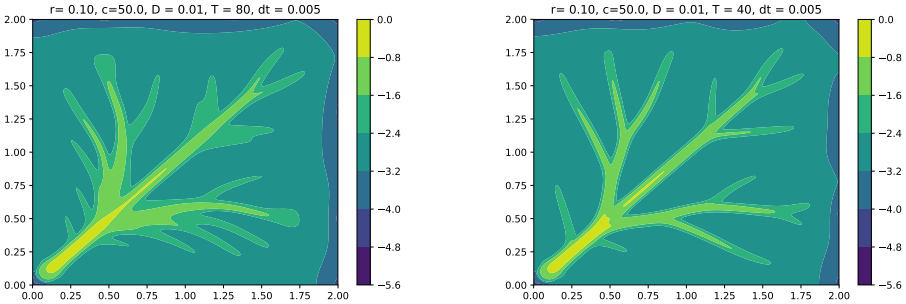

(a) $t = 20$ (b) $t = 40$

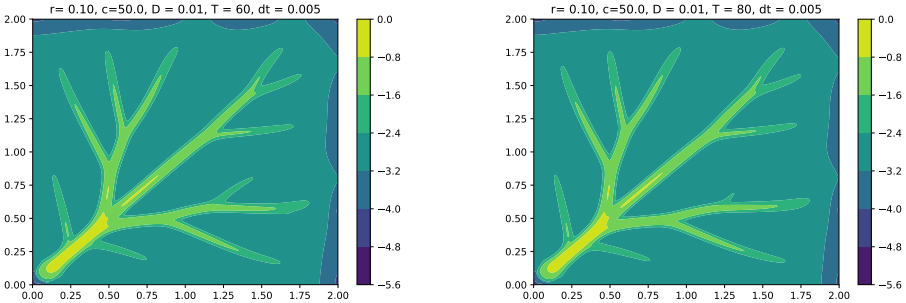

(c) $t = 60$ (d) $t = 80$

Figure 7: Example 4.3 computed by the semi-implicit solver: the flux u defined in(4.3) at different times $t = 20, 40, 60, 80$. It can be seen that the leaf grows and finally achieves a tree-like structure.

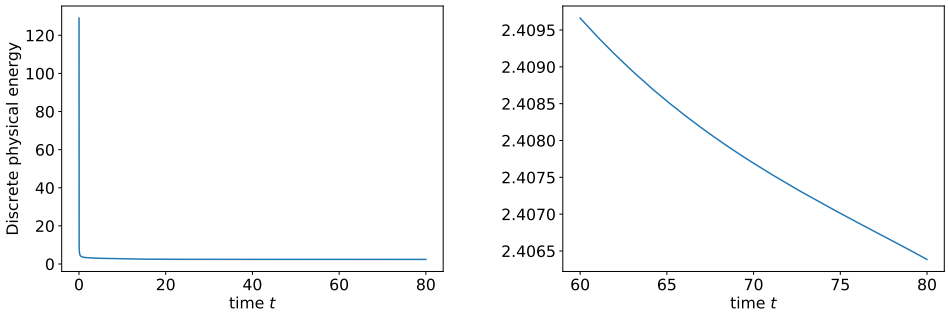

(a) Discrete physical energy for $t \leq 80$ (b) Zoom in to the tail for $60 \leq t \leq 80$

Figure 8: Example 4.3 computed by the semi-implicit solver: The discrete physical energy decays all the time, and it can be seen in the zoom-in figure (on the right) that it keeps the decay behavior even if the first two decimal places no longer change.

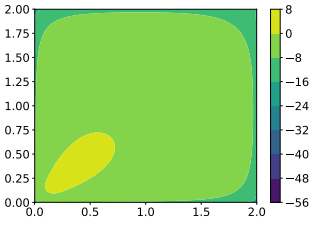

(a) leaf structure $|m|^2$ in log-scale

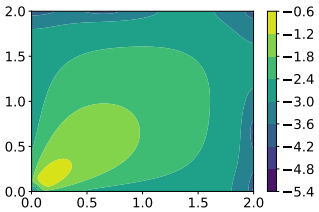

(b) flux u in log-scale

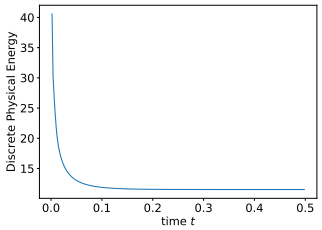

(c) Discrete Physical energy versus time

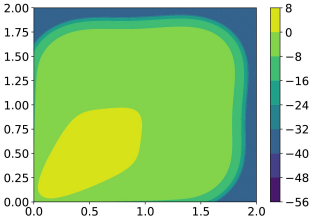

(d) leaf structure $|m|^2$ in log-scale

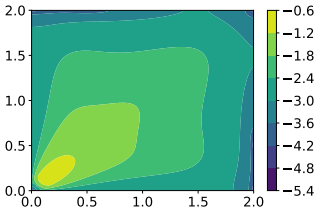

(e) flux u in log-scale

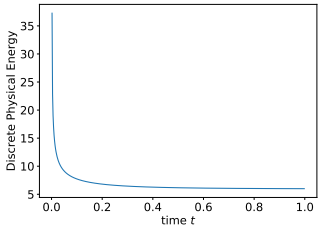

(f) Discrete Physical energy versus time

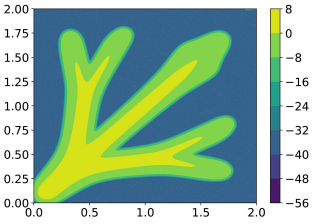

(g) leaf structure $|m|^2$ in log-scale

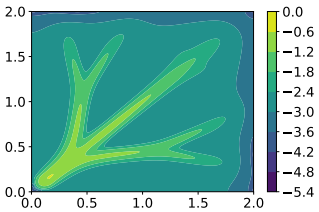

(h) flux u in log-scale

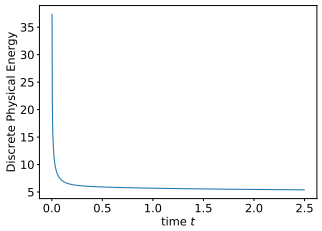

(i) Discrete Physical energy versus time

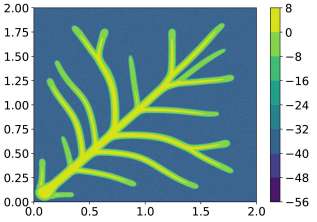

(j) leaf structure $|m|^2$ in log-scale

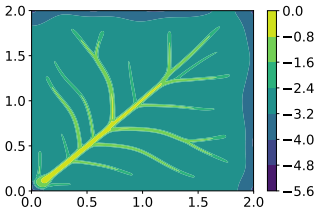

(k) flux u in log-scale

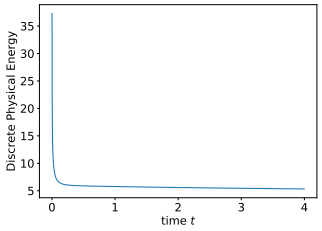

(l) Discrete Physical energy versus time

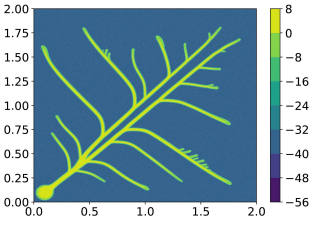

(m) leaf structure $|m|^2$ in log-scale

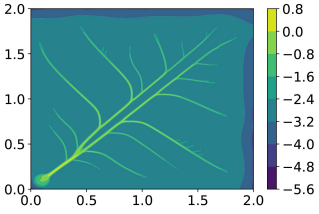

(n) flux u in log-scale

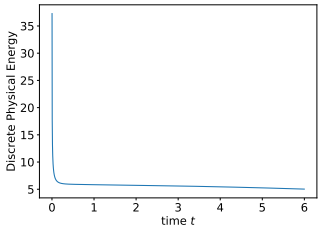

(o) Discrete Physical energy versus time

Figure 9: Example 4.4 computed by the semi-implicit solver for various D till $T = 40$. From first row to the last row, the values of D are $0.5, 0.1, 0.02, 0.005$ and 0.002, respectively. It can be seen that the smaller the diffusion coefficient is, the more detailed the network structure becomes.

Example 4.5 (Varying spatial mesh size)**.** In this example, we test the semi-implicit scheme with different spatial mesh size. In this example, we first take asymmetric initial datum as in Fig. 5, and denote the non-zero region are Ω_0. We take with a small perturbation $\sim 0.1\text{Uniform}(\Omega_0)$ on the initial datum in the region Ω_0. We take $D = 0.01$ and the number of grid points in each spatial direction as 500, 800 and 1000. It can been see in Fig 10, the differences resulting from the varying of the spatial mesh size are of small magnitude as can be seen in both the log scale and the regular scale.

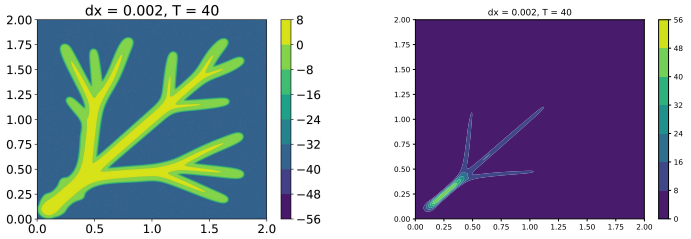

(a) leaf structure $|m|^2$ in log-scale

(b) $|m|^2$

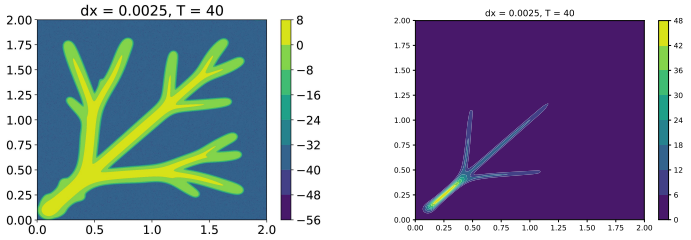

(c) leaf structure $|m|^2$ in log-scale

(d) $|m|^2$

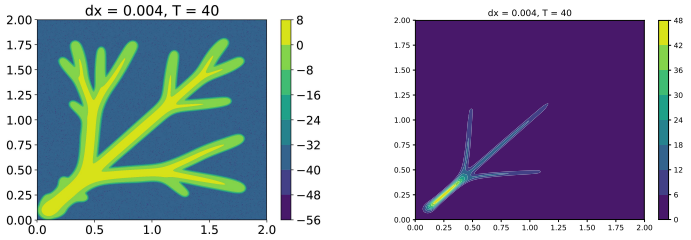

(e) leaf structure $|m|^2$ in log-scale

(f) $|m|^2$

Figure 10: Example 4.5 (asymmetric initial datum) computed by the semi-implicit solver for $D = 0.01$ till $T = 40$ for various grid points in each spatial direction. The first row: 1000 by 1000; the second row 800 by 800; the third row: 500 by 500. Though the pattern seem a bit different in the log scale, it can be seen from the plots that the differences between the three results are in fact minor in the normal scale.

Now, we take symmetric initial data and symmetric source S. For $\gamma = 0.75, D = 0.01$, the solutions are computed until $T = 20$ using the number of grid points in each spatial direction as 500, 800 and 1000, respectively. It can been see in Fig 12, the pattern seems symmetric, and varying different mesh sizes does not seem to break the symmetry. It can be seen in the middle

column of Fig. 12 that the differences resulting from the change of the grid size are minor, which are more clearly illustrated in the log-scale plots (first and last columns) that the difference is of order 1e−4 marked as dark yellow in the color bar.

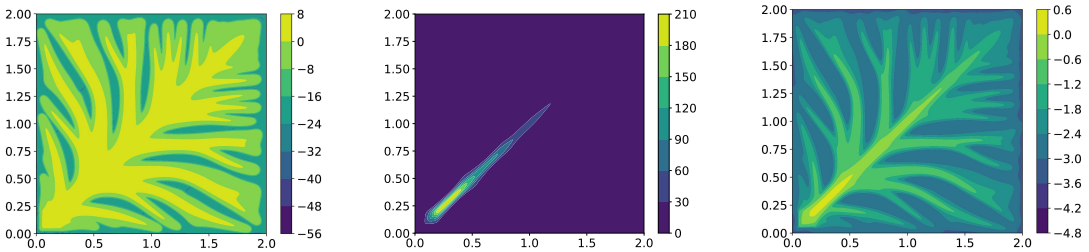

(a) leaf structure $|m|^2$ in log-scale (b) $|m|^2$ (c) flux u in log-scale

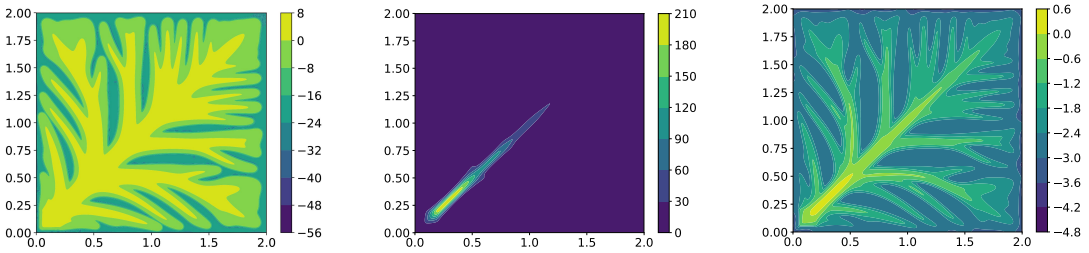

(d) leaf structure $|m|^2$ in log-scale (e) $|m|^2$ (f) flux u in log-scale

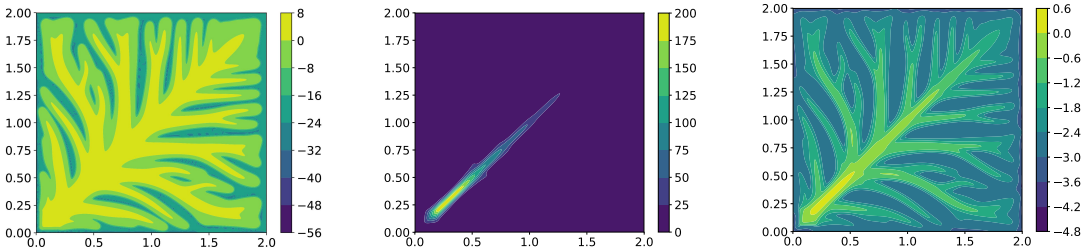

(g) leaf structure $|m|^2$ in log-scale (h) $|m|^2$ (i) flux u in log-scale

Figure 11: Example 4.5 (symmetric initial datum) computed by the semi-implicit solver for $D = 0.01$ till $T = 20$ for various grid points in each spatial direction. The first row: 1000 by 1000; the second row 800 by 800; the third row: 500 by 500. The symmetry of the patterns is not broken by varying of the mesh size.

Example 4.6 (Asymmetric Grids)**.** An interesting phenomenon been pointed out in [14] that for asymmetric grids, the solution could form an asymmetric pattern even with symmetric initial data and source. In this last example, we change to an asymmetric grids, namely, $dx \neq dy$. We consider the symmetric initial data as in Example 4.5 with $\gamma = 0.75$ and $D = 0.01$, but use 500 grid points in x direction while 800 grid points in y direction. As can be see in Fig. 12, the pattern becomes asymmetric in the log-scale plot, but in fact in the regular scale the solution

does not seem to differ much from the results of symmetric grids as plotted in Fig. 11 middle column. We point out that just as the checkerboard problem in computational fluid dynamics, to avoid some potential instability caused by the "natural grids", the choice of grids should certainly be carefully designed. Here we used the staggered grids, and a better gridding strategy for both finite difference and finite element schemes of this model is a very interesting problem, which is left for future study.

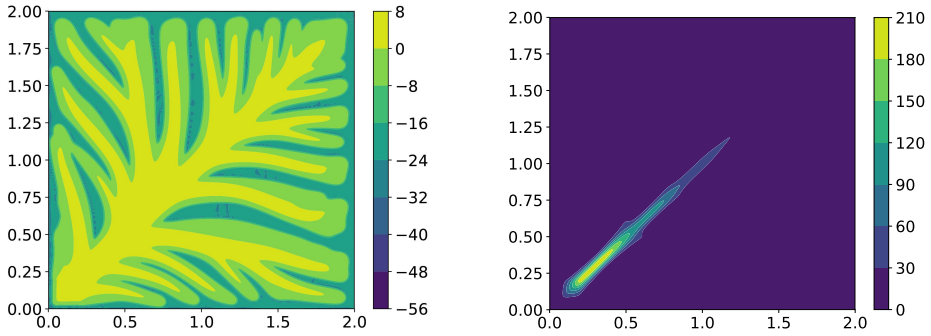

(a) $|m|^2$ in log-scale

(b) $|m|^2$

Figure 12: Example 4.6 symmetric initial data with asymmetric grids $dx \neq dy$. The pattern becomes asymmetric as well. But as can be seen in the regular scale (on the right), the solution does not differ much from the results of symmetric grids (see Fig. 11 middle column).

5 Conclusion

In this work, we propose two possible approaches to the Cai-Hu model for biological transport networks – the fully implicit treatment and a semi-implicit approach. While the fully implicit one is proven to be unconditionally stable in 1D, it results in a nonlinear algebraic system that could be difficult and costly to implement in higher dimension, and convergence of the Newton solver remains unclear. The semi-implicit scheme avoids the Newton iteration, but has a stability constraint on time step which depends on some coefficients of the equation (still independent of the mesh size though). For the 2D model, the semi-implicit scheme is of more practical potential, since it only deals with linear algebraic problems by inverting positive definite matrices that can be solved efficiently by CG or PCG even in higher dimensions. Our numerical examples show the stabilities and energy decay of both schemes.

References

[1] G. Albi, M. Artina, M. Foransier, and P. A. Markowich. Biological transportation networks: Modeling and simulation. *Analysis and Applications*, 14(01):185–206, 2016.

[2] G. Albi, M. Burger, J. Haskovec, P. Markowich, and M. Schlottbom. *Continuum Modeling of Biological Network Formation*, pages 1–48. Springer International Publishing, Cham, 2017.

[3] S. Bohn and M. O. Magnasco. Structure, scaling, and phase transition in the optimal transport network. *Phys. Rev. Lett.*, 98:088702, Feb 2007.

[4] M. Burger, J. Haskovec, P. Markowich, and H. Ranetbauer. A mesoscopic model of biological transportation networks. *ArXiv e-prints*, May 2018.

[5] S. D. Conte and C. De Boor. *Elementary Numerical Analysis: An Algorithmic Approach*. Classics in Applied Mathematics. Society for Industrial and Applied Mathematics (SIAM, 3600 Market Street, Floor 6, Philadelphia, PA 19104), 2018.

[6] F. Corson. Fluctuations and redundancy in optimal transport networks. *Phys. Rev. Lett.*, 104:048703, Jan 2010.

[7] P. Dimitrov and S. W. Zucker. A constant production hypothesis guides leaf venation patterning. *Proceedings of the National Academy of Sciences*, 103(24):9363–9368, 2006.

[8] Q. Du and W. Zhu. Analysis and applications of the exponential time differencing schemes and their contour integration modifications. *BIT Numerical Mathematics*, 45(2):307–328, 2005.

[9] Q. Du and W.-x. Zhu. Stability analysis and application of the exponential time differencing schemes. *Journal of Computational Mathematics*, pages 200–209, 2004.

[10] X. Feng, H. Song, T. Tang, and J. Yang. Nonlinear stability of the implicit-explicit methods for the allen-cahn equation. *Inverse Problems & Imaging*, 7(3), 2013.

[11] J. Haskovec, L. M. Kreusser, and P. Markowich. ODE and PDE based modeling of biological transportation networks. *ArXiv e-prints*, May 2018.

[12] J. Haskovec, L. M. Kreusser, and P. Markowich. Rigorous Continuum Limit for the Discrete Network Formation Problem. *ArXiv e-prints*, Aug. 2018.

[13] J. Haskovec, P. Markowich, and B. Perthame. Mathematical analysis of a pde system for biological network formation. *Communications in Partial Differential Equations*, 40(5):918–956, 2015.

[14] J. Haskovec, P. Markowich, B. Perthame, and M. Schlottbom. Notes on a pde system for biological network formation. *Nonlinear Analysis*, 138:127 – 155, 2016. Nonlinear Partial Differential Equations, in honor of Juan Luis Vzquez for his 70th birthday.

[15] D. Hu and D. Cai. Adaptation and optimization of biological transport networks. *Phys. Rev. Lett.*, 111:138701, Sep 2013.

[16] D. Hu and D. Cai. Adaptation and optimization of biological transport networks. *Phys. Rev. Lett.*, 111:138701, Sep 2013.

[17] E. Katifori, G. J. Szöllősi, and M. O. Magnasco. Damage and fluctuations induce loops in optimal transport networks. *Phys. Rev. Lett.*, 104:048704, Jan 2010.

[18] A. Koller and G. Kaley. Endothelial regulation of wall shear stress and blood flow in skeletal muscle microcirculation. *American Journal of Physiology-Heart and Circulatory Physiology*, 260(3):H862–H868, 1991. PMID: 2000980.

[19] M. F. Laguna, S. Bohn, and E. A. Jagla. The role of elastic stresses on leaf venation morphogenesis. *PLOS Computational Biology*, 4(4):1–10, 04 2008.

[20] D. Lu and G. S. Kassab. Role of shear stress and stretch in vascular mechanobiology. *Journal of the Royal Society Interface*, 8(63):1379–1385, Oct. 2011.

[21] C. D. Murray. The Physiological Principle of Minimum Work: I. The Vascular System and the Cost of Blood Volume. *Proceedings of the National Academy of Sciences of the United States of America*, 12(3):207–214, Mar. 1926.

[22] T. Nelson and N. Dengler. Leaf vascular pattern formation. *The Plant Cell*, 9(7):1121–1135, 1997.

[23] U. Pohl, J. Holtz, R. Busse, and E. Bassenge. Crucial role of endothelium in the vasodilator response to increased flow in vivo. *Hypertension*, 8(1):37–44, 1986.